A Brief Review of Compressive Sensing Applied to Radar

Joachim Ender

Fraunhofer-Institut für Hochfrequenzphysik und Radartechnik FHR
Fraunhoferstrasse 20, 53343 Wachtberg, Germany
email: joachim.ender@fhr.fraunhofer.de

Abstract: *In this paper we give a brief review of compressive sensing (CS) applied to radar. Though CS theory has been introduced only a few years ago (in 2006, see e. g. [1]), it today manifests as a kind of revolution in signal processing and sensor systems. We will discuss some properties of CS radar and present a few examples. It is also a concern of the author to point to some limitations and shortcomings if CS is 'blindly' applied with great enthusiasm to any radar problem. The time has come to deliberate when CS will be an advantage and when 'oldfashioned' methods should better be applied.*

1. Introduction

Today sensor-systems like radar are based on digital signal processing to a growing degree. The analogue-to-digital converter moves up more and more to the analogue frontend. The sampling rate in general still is based on the sampling theorems developed in the 1920^{th} and 1930^{th} by Harry Nyquist, Vladimir Aleksandrovich Kotelnikow, and other 'patriarchs' of sampling theory. For modern broadband systems the adherence to Nyquist sampling leads to a tremendous flood of data, and a large number of single elements for a receiving array. Many attempts have been undertaken to reduce this data flood as predecessors of compressive sensing (CS). Nevertheless, for the first time the latter has presented a round theory for sub-Nyquist sampling.

2. Basic ideas of compressive sensing

In the 21^{th} century a new type of sampling theorems has been developed, summarized under the term 'compressed sensing'. The class of admitted signals is restricted to *sparse* or *compressible* signals. In the scope of our paper the word 'signal' often will be replaced by *scene*, i.e. that what we want to observe, image or reconstruct. Experience shows that most scenes in our environment are more or less compressible or even sparse. It is evident that in everyday life compression techniques often come across, for photos, videos or music showing the compressibility of real life signals. The same is true for many radar applications.

The new theory of CS is well founded on a solid mathematical basis. It joins the description of sparse or compressible scenes with sparse sensing techniques, contributes algorithms for reconstruction and presents mighty, well proven theorems. It provides a new glance at the world of signal processing and sensor techniques. The number of papers on CS (and CS applied to

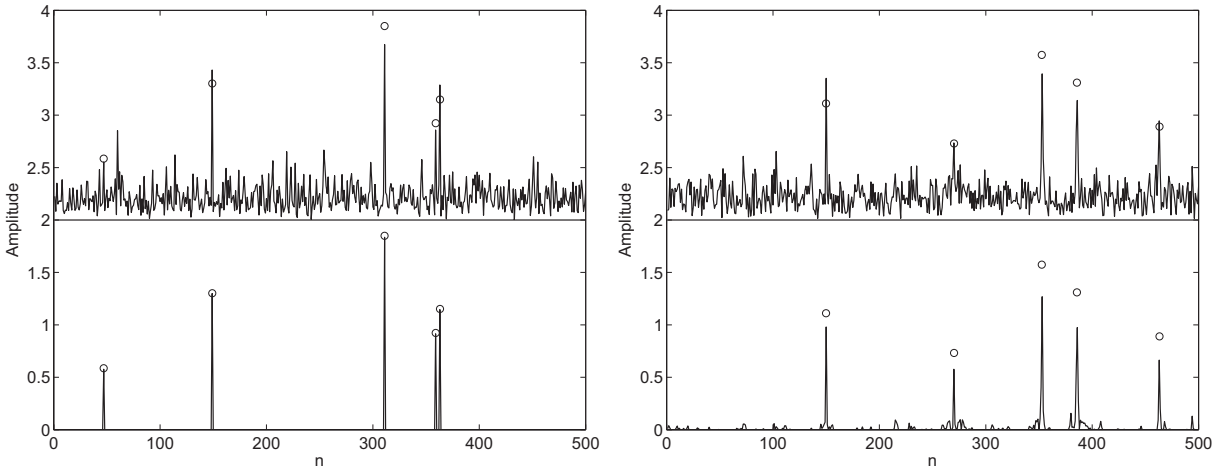

Figure 1: *Left: Example for reconstructions of a simulated scene with scatterers at the grid points. Top left: reconstruction with matched filter. Bottom left: reconstruction with ℓ_1-minimization. The markers indicate the true values. $N = 500, M = 100, S = 5$, noise = -30dB, partial Fourier matrix. Right: Example for reconstruction of a simulated scene with points between the grids. The positions are uniformly randomly chosen. Top right: reconstruction with matched filter. Bottom right: reconstruction with ℓ_1-minimization. The markers indicate the true values. The parameters are the same as before.*

radar) is exploding nearly exponentially. But still there are only a few papers dealing with real world radar data.

Compressive sensing techniques generally deal incomplete linear equation systems of the type

$$\mathbf{y} = \mathbf{A}\mathbf{x} \tag{1}$$

where the N-dimensional coefficient vector $\mathbf{x}$ describes the *scene*, the M-dimensional vector $\mathbf{y}$ collects the *measurements* obtained by a linear sensor and $\mathbf{A}$ is an $M \times N$ matrix - the *sensing matrix* - characterizing how the coefficient vector is mapped to the measurements. The vectors and matrices may be real or complex valued. Compressive sensing assumes that $M < N$, hindering that Eq. 1 can simply be inverted to reconstruct $\mathbf{x}$ from the measurements. A vector $\mathbf{x}$ is called S*-sparse* if at most S of its coefficients are unequal to zero, and *compressible* if $\|\mathbf{x} - \mathbf{x}(S)\|$ decreases quickly to zero with growing S, when $\mathbf{x}(S)$ denotes the best S-sparse approximation of $\mathbf{x}$.

There is a variety of algorithms aiming to reconstruct $\mathbf{x}$ from the deterministic measurements $\mathbf{y} = \mathbf{A}\mathbf{x}$ or the noisy measurements $\mathbf{y} = \mathbf{A}\mathbf{x} + \mathbf{n}$ under the assumption that $\mathbf{x}$ is sparse. Well known are the *Basis Pursuit*, minimizing the ℓ_1-norm $\|\mathbf{x}\|_1$ subject to $\mathbf{y} = \mathbf{A}\mathbf{x}$, the *Basis Pursuit Denoising* [2] minimizing $\|\mathbf{x}\|_1$ subject to $\|\mathbf{y} - \mathbf{A}\mathbf{x}\|_2 \leq \sigma$, or equivalently: $\|\mathbf{x}\|_1 + \lambda\|\mathbf{y} - \mathbf{A}\mathbf{x}\|_2$, the *Orthogonal Matching Pursuit* (OMP)[3] and the *Compressive Sampling Matched Pursuit* (CoSaMP) [4]. For the mode of operation of these algorithms, the reader is referred to literature.

It has been shown that under certain conditions on the sensing matrix exact (for the noise-free case) or robust (for the noisy case) reconstruction is guaranteed, if the number M of measurements is larger or equal to an expression depending on N, S and a quantity describing a specific

property of the sensing matrix. One of these measures is the *Restricted Isometry Constant* given by the minimum number δ with $(1-\delta)\|\mathbf{x}\|_2^2 \leq \|\mathbf{A}\mathbf{x}\|_2^2 \leq (1+\delta)\|\mathbf{x}\|_2^2$ for all S-sparse vectors $\mathbf{x}$, assuring that measurements $\mathbf{A}\mathbf{x}$ and $\mathbf{A}\mathbf{x}'$ are different, if only the S-sparse vectors $\mathbf{x}$ and $\mathbf{x}'$ are sufficiently separated. Since this *Restricted Isometry Property* (RIP) is difficult to proof for a concrete matrix, a theory has been developed regarding classes of statistical sensing matrices, showing that e.g. RIP is fulfilled with a probability close to 1. For instance it was shown that for Gaussian or Rademacher random matrices will have the (S,δ)-RIP with with high probability, if $M = \mathcal{O}\left(\frac{S\log\frac{N}{S}}{\delta^2}\right)$. For one type of statistical sensing matrices generated by selecting M rows of the complete $N \times N$ Fourier matrix by random, some examples are presented in this paper.

3. Radar applications of CS

There are many papers about application of CS to various radar tasks. The most elementary task is *pulse compression*, treated in a large number of papers, where sparse sampling can be applied in the fast time domain as well as in the frequency domain. An efficient method is to transmit a set of frequencies instantaneously [5, 6]. The optimization of the waveforms for CS is regarded e.g. in [7, 8], orthogonal frequency division multiplexing (OFDM) waveforms in [9]. *Aerospace multi-channel MTI* is an interesting situation where the space of scene points is extended by the dimension 'radial velocity'. The clutter returns gather at the subspace $v = 0$ while moving targets are represented by sparse points in the volume [10].

A great attention has been directed to *multiple-input/multiple-output (MIMO)* radar systems [11, 12]. This situation well fitted to CS reconstruction, since the signals are related to all Tx/Rx pairs which in general lead to a non-uniform thinned sampling in range and angles. *Passive coherent location (PCL)* is a special case of a MIMO radar where the waveforms and the positions of the transmitters cannot be influenced by the user [13],[14].

The application of CS to *Synthetic Aperture Radar (SAR)* [15, 16] may be problematic, first because of the possibly not given sparsity of the reflectivity, and secondly because of the tremendous numerical effort needed if larger images shall be processed. On the other hand, CS applied to *SAR tomography* is really a great example for a reasonable CS use [17, 18, 19]. While the SAR images for different pathes of an earth observation satellite are conventionally generated in range and azimuth, the reflectivity in the third dimension - here: the elevation angle - is reconstructed via CS. Since normally in one range-azimuth pixel only one elevation angle is occupied by scatterers, in the case of layover also reflections from two or more elevation angles can be present. The scene is naturally sparse in the third dimension. The application of CS to *ISAR imaging* [20, 21] is promising, especially since the number of pixels can be limited and the objects often show sparse reflections.

Many attempts have also been undertaken to process *ultra-wide-band (UWB) radar* data by CS algorithms, often in the application to *through-the-wall radar* [22, 23, 22] and *ground penetrating radar* [24, 25, 26]. The latter is particularly interesting because of the unknown permittivity of the ground. Even for the retrieval of the refractivity field from a network of *weather radars*

CS has been applied [27].

Definitely radar engineers are interested not only in the probability of a perfect reconstruction, but also in the probability distribution of the reconstructed values, optimum test statistics to be applied to them and the probabilities of false alarm and detection. Many of these questions are answered in [28, 29, 30].

4. Radar scenes, sparsity and measurements

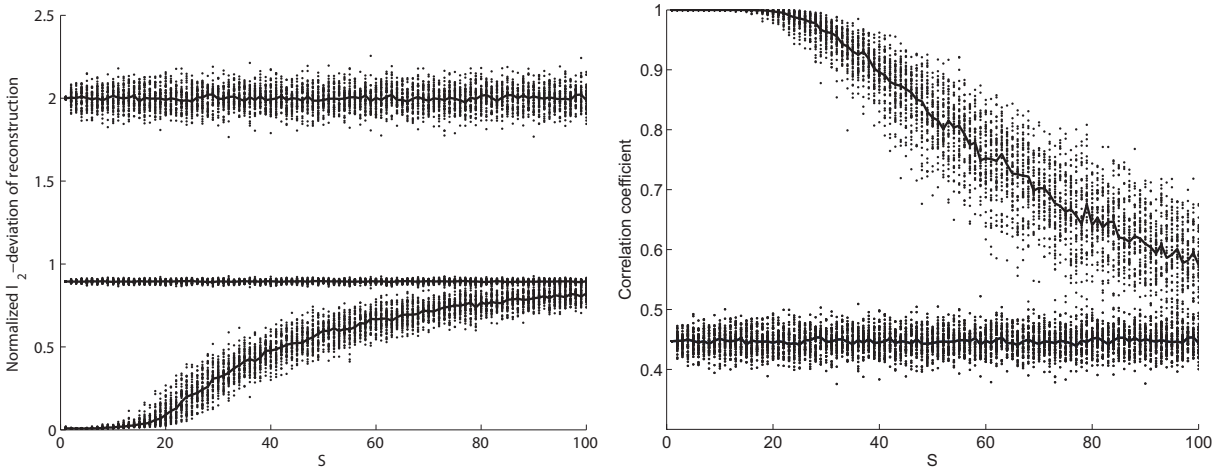

Figure 2: *Left: Reconstruction quality of three methods as functions of the sparsity S, measured as the quotient between the ℓ_2-norm of the deviation between scene and reconstructed scene and the ℓ_2-norm of the scene. The points are single simulation results and the lines connect the medians for the respective simulations. The lowest curve relates to the noisy basis pursuit, the middle curve to the energy-minimization and the upper curve to matched filtering. $N = 500, M = 100$, noise = -30dB, partial Fourier matrix. Right: Reconstruction quality measured as the correlation coefficient between the scene and the reconstructed scene. The upper curve relates to the noisy basis pursuit, the lower curve to matched filter reconstruction, which produces in this case the same values as the energy-minimization.*

To explore a scene with a radar sensor, in general we want to get information about the reflectivity $\rho(\omega)$ over a set $\omega \in \Omega$ of scene points which may be geometrical positions or also points in a higher dimensional space including velocities, polarizations and so on. To get the information, radar parameters ξ (frequencies, antenna positions, platform position, ...) are varied and measurements are taken for each used ξ [5]. To process the data, a signal model $s(\xi;\omega)$ is needed describing the expected signal for a scatterer with normalized reflectivity at ω if the radar parameter ξ is used. To apply CS we need to discretize the scene points $\omega_1, \ldots, \omega_N$ as well as the measuring parameters $\xi_1, \ldots, \xi_M$ leading to an N-dimensional reflectivity vector $\boldsymbol{\rho} = (\rho(\omega_1), \ldots, \rho(\omega_N))^t$, a measurement vector $\mathbf{y} = (y(\xi_1), \ldots, y(\xi_N))^t$ and an $M \times N$ model signal matrix $\mathbf{S}$, $S_{mn} = s(\xi_m;\omega_n)$.

If the radar sensor and the reflection mechanisms can be assumed to be linear, the mapping between the reflectivity and the noise-less measurements are given by $\mathbf{y} = \mathbf{S}\boldsymbol{\rho}$ and the noisy measurements by $\mathbf{y} = \mathbf{S}\boldsymbol{\rho} + \mathbf{n}$ where $\mathbf{n}$ is a realization of the random vector $\mathbf{N}$. The reflectivity

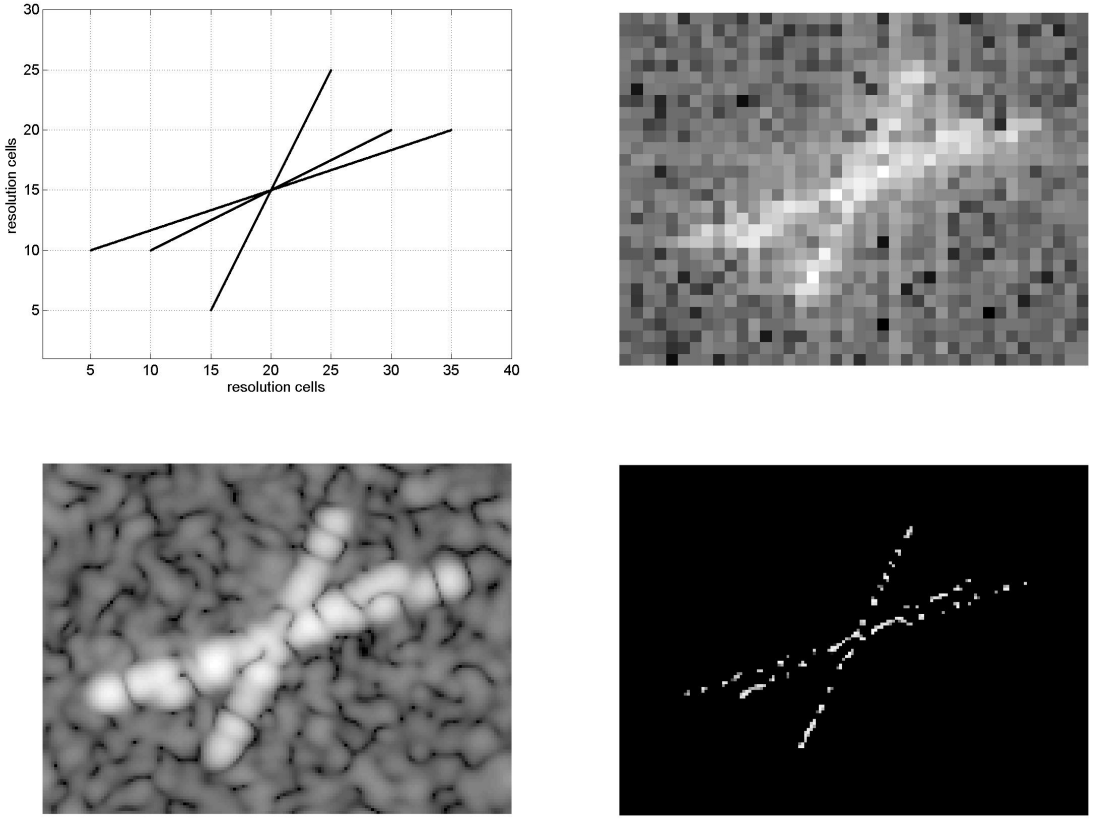

Figure 3: *Simulation of the imaging of three cutting lines. Left top: the original scene, scaled in resolution cells. Right top: FFT image without window, not oversampled. Left bottom: Hamming-windowed FFT with an oversampling factor of 4 in both directions. Right bottom: CS reconstruction with the same zoom factor. Resolution cells x-direction = 30, Resolution cells y-direction = 40, zoom = 4×4, $N = 19200$, $M = 1200$, signal-to-noise ratio of the strongest scatterer: 33 dB. Dynamic of the images: 30 dB.*

$\boldsymbol{\rho}$ may be expressed by a complete system of basis vectors $\mathbf{b}_1, \ldots, \mathbf{b}_N$ by $\boldsymbol{\rho} = \sum_{n=1}^{N} x_n \mathbf{b}_n$, or in matrix notation $\boldsymbol{\rho} = \mathbf{B}\mathbf{x}$ where $\mathbf{B}$ is the matrix composed of the column vectors $\mathbf{b}_n$. Henceforth, the scene is called S*-sparse* if a *representation basis* $\mathbf{B}$ can be found for which the coefficient vector $\mathbf{x}$ is S-sparse.

Now the measuring equation can be written as $\mathbf{y} = \mathbf{S}\boldsymbol{\rho} = \mathbf{S}\mathbf{B}\mathbf{x} = \mathbf{A}\mathbf{x}$ with $\mathbf{A} = \mathbf{S}\mathbf{B}$ and we are back at the original sparse reconstruction problem. In most of the cases, we are looking for 'spiky' reflectivities, i.e. $\boldsymbol{\rho}$ itself is sparse, the identity representation basis $\mathbf{B} = \mathbf{I}$ can be used, and $\mathbf{x}$ is identical to $\boldsymbol{\rho}$.

The collection of the column vectors of $\mathbf{A}$ is called *dictionary*, since to each of the possible positions in the vector $\mathbf{x}$ there corresponds a description, namely the corresponding column vector of $\mathbf{A}$. A dictionary can be extended by adding scene points related to different properties, for instance reflectivity characteristics of the scatterers, building a broader base for classification.

4.1. Example: range profile reconstruction

As a leading example we regard a radar illuminating an object with harmonic waves with wave numbers $k = 2\pi/\lambda$ where λ is the wave length. A scatterer at range r with normalized reflectivity will lead to the receive signal in baseband $s(k;r) = \exp\{-j2kr\}$. Obviously, in this case the scene points ω can be identified with the range values r and the measuring parameters ξ with the wave number k. Introducing a grid of range values $r_1, \ldots, r_N$ and a set of wavenumbers $k_1, \ldots, k_N$, the model signal matrix results in $\mathbf{S} = (s(k_m; r_n))_{m=1\ldots M, n=1\ldots N}$. If a range grid $r_n = r_0 + n\Delta r$ and a wavenumber grid $k_m = k_0 + m\Delta k$ are used and if $\Delta k = 2\pi/(N\Delta r)$ is chosen to fulfill the Nyquist condition, after compensation of the start range r_0 and the start wave number k_0 we get for $M = N$ the complete discrete Fourier matrix $\mathbf{S} = (\exp\{-j2\pi mn/N\})_{m=1\ldots N, n=1\ldots N}$.

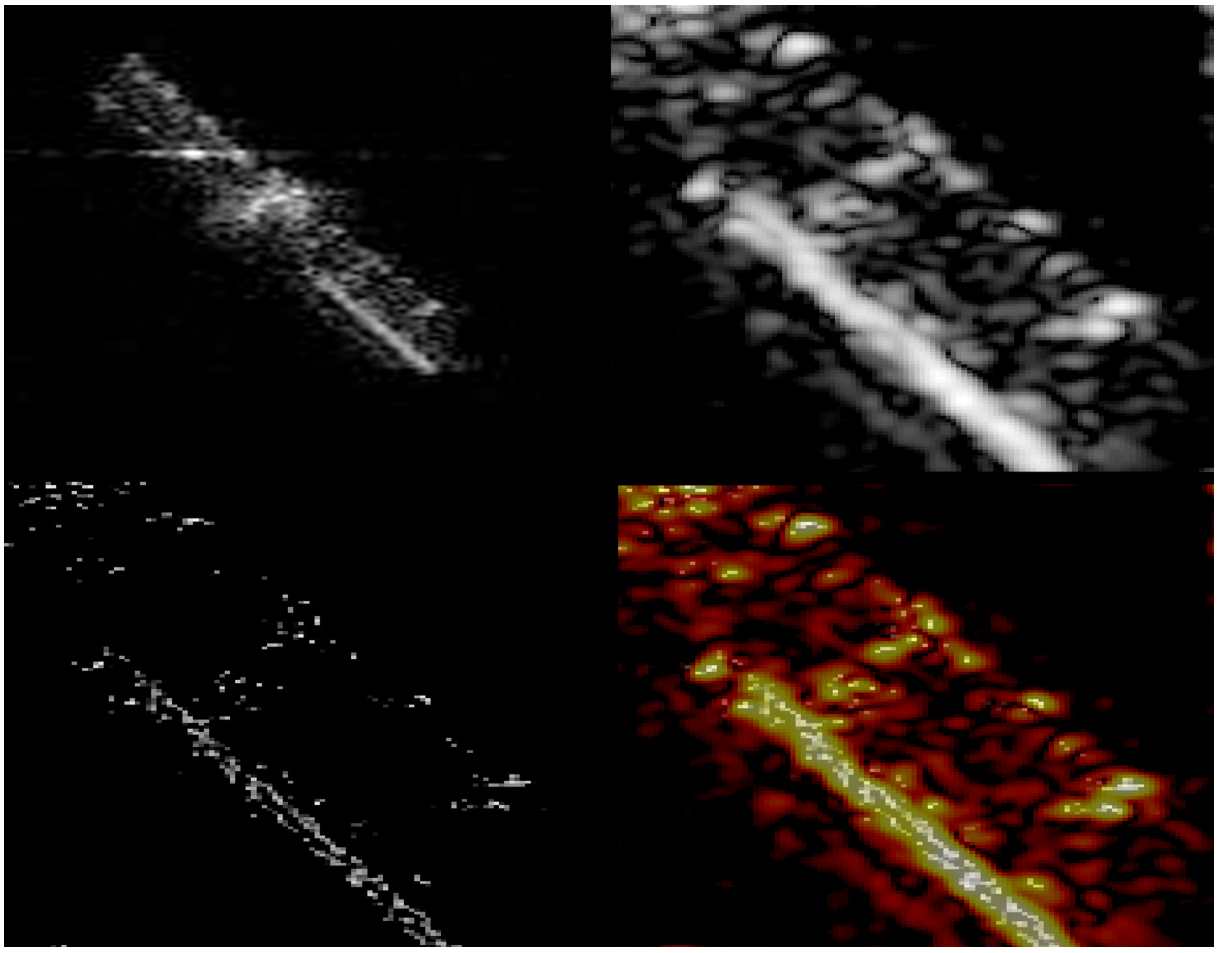

Figure 4: *ISAR images of a satellite observed with the Fraunhofer-radar 'TIRA'. Left top: ISAR image of the whole satellite. Right top: Hamming-windowed FFT image of a detail with an oversampling factor of 2.8 in both directions. Left bottom: CS-image with the same oversampling factor. Right bottom: Overlay of Hamming- and CS-image. N = 18055, M = 2296*

Fig. 1 shows the result of CS-reconstruction if only a random selection of M wave-numbers out of N is used. The result is really striking and inspiring! The spiky reflectivity distribution is

nearly perfectly reconstructed though noise was added. A first general question is arising: How robust are the algorithms against deviations from the model $\mathbf{y} = \mathbf{A}\mathbf{x}$? There are two sources of error: The first is additive noise which effectively can be taken into account by using the basis pursuit denoising. The second is a deviation of the signals from the signal model underlying the assumed matrix $\mathbf{A}$. These are due to imperfect calibration, but also to a deviation of the real position (here: the real range) from the specified grid. The latter situation is simulated (see Fig. 1 right) for ranges randomly chosen in the range interval. Obviously, the result is still considerable though a kind of sidelobes appear. There exist methods to perform a fine estimation of the positions and to reconfigure the grid with nearly optimum reconstruction results.

4.2. Is CS better than conventional methods like matched filtering?

If $\mathbf{y} = x\mathbf{a} + \mathbf{n}$ where $\mathbf{n}$ is a realization of a random vector $\mathbf{N}$ with expectation $\mathbf{0}$ and covariance matrix $\sigma^2\mathbf{I}_M$, the maximum signal-to-noise ratio of a linear estimator of x is achieved by the *matched filter* $\widehat{x}_{mf} = \frac{\mathbf{a}^H\mathbf{y}}{\|\mathbf{a}\|_2^2}$. This is also the best unbiased estimator of x, if $\mathbf{N}$ is Gaussian distributed. But this is only valid if only one coefficient is present! For our model $\mathbf{y} = \mathbf{A}\mathbf{x} + \mathbf{n}$ the matched filter can also be applied: $\widehat{\mathbf{x}}_{mf} = \mathbf{A}^H\mathbf{y}$; Here the columns of $\mathbf{A}$ are normalized to ℓ_2 unit vectors, i.e. diag $\left(\mathbf{A}^H\mathbf{A}\right) = \mathbf{I}_N$ without loss of generality. We remark that this technique is applied in various fields of radar signal processing, as pulse compression, beam forming, SAR image generation, ... Is it still optimum, if $N > 1$? First, it is no longer unbiased for any vector $\mathbf{x}$ with at least two elements unequal to zero, since $E[\widehat{\mathbf{x}}_{mf}] = \mathbf{A}^H\mathbf{A}\mathbf{x}$ and $\mathbf{A}^H\mathbf{A}$ cannot be the unit matrix for $N > M$. For randomly chosen Fourier vectors the expectation of the ℓ_2-norm of the bias $\|E[\widehat{\mathbf{x}}_{mf}] - \mathbf{x}\|^2$ is calculated to $\frac{N-M}{M}\|\mathbf{x}\|_2^2$ independent on the the structure of $\mathbf{x}$.

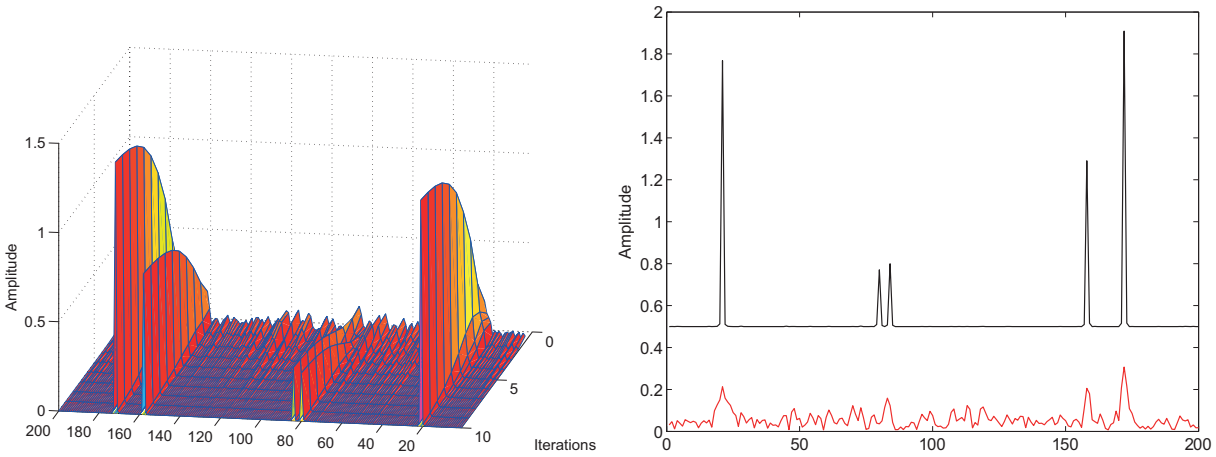

Figure 5: *Range profile reconstruction for a spiky scene corrupted by a quadratic phase error. N = 200, M = 50, S = 5. Left: The history of reconstruction over 10 iterations. Right: start and final estimation of the amplitude. The latter was upshifted by 0.5 to improve the clarity.*

A better estimation quality in this sense is got by the classical estimator $\widehat{\mathbf{x}}_{em} = \mathbf{A}^\dagger\mathbf{y}$ where $\mathbf{A}^\dagger = \mathbf{A}^H\left(\mathbf{A}\mathbf{A}^H\right)^{-1}$ is the pseudo-inverse of $\mathbf{A}$. This estimator is the solution of the minimization of $\|\mathbf{x}\|_2^2$ subject to $\mathbf{y} = \mathbf{A}\mathbf{x}$ analogue to the ℓ_1-minimization. Its expectation is equal to $\mathbf{P}_A\mathbf{x}$

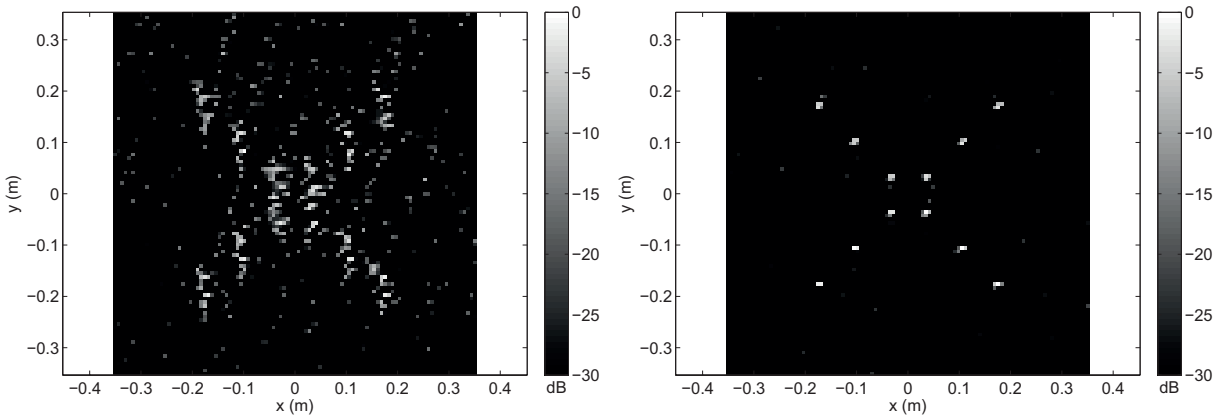

Figure 6: *Left: CS image of a simulated object with phase errors. Right: After phase correction using sparse represenation and phase gradient estimation*

where $\mathbf{P}_A = \mathbf{A}^H \left(\mathbf{A}\mathbf{A}^H\right)^{-1} \mathbf{A}$ is the projector on the M-dimensional subspace spanned by the rows of $\mathbf{A}$. The expectation of the norm-squared bias $\mathbf{x}^H(\mathbf{I} - \mathbf{P}_A)\mathbf{x}$ is equal to $\frac{N-M}{N}\|\mathbf{x}\|_2^2$ for the partial Fourier case.

In Fig. 2 left the MMS deviation of the estimated from the true $\mathbf{x}$ as obtained by a simulation series is plotted against the sparsity degree. We recognize that for the matched filter and energy minimization estimators the errors are independent on S and close to the expected values $\sqrt{\frac{N-M}{M}}(= 2)$ and $\sqrt{\frac{N-M}{N}}(= 0.89)$, respectively. These large errors are no wonder since without further assumptions about $\mathbf{x}$ a good estimate based on the underdetermined equation system is impossible! However, we daily apply this method, also with $N > M$, e.g. for Fourier analysis or SAR imaging with a grid finer than the resolution cells, of for beamforming with a thinned array, and so on.

Much more convincing is the result for CS reconstruction! The error is nearly zero as long as S is small enough, in the example around $S = 10$, but also for larger S the advantage with respect to the two classical methods is still large. Similar conclusions can be gained by looking at the correlation coefficient between scene and reconstructed scene, see Fig. 2 right.

The answer to the question 'Is CS better than conventional algorithms?' in this light should be answered with 'Yes, it is!'. At least if the a priori assumption of the scene-sparsity is fulfilled.

5. Can CS produce super-resolution?

If the grid carrying the scene has a spacing smaller than the Rayleigh resolution cell, there is hope arising that CS reconstruction could show *super-resolution* properties [31, 32]. The number of measurements M may be chosen according to the Nyquist sampling, while the number N of grid points is increased by a certain zoom-factor. On the other hand, the incoherency of the sensing matrix is reduced since the model signals for scene points separated less than a

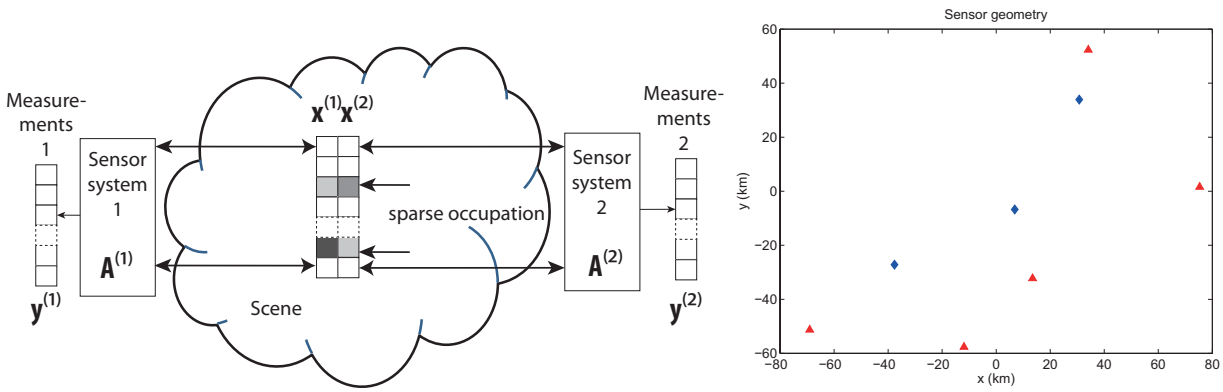

Figure 7: *Left: Illustration of sensing a block sparse scene with mutually non-coherent sensors. Right: Sensor geometry used for simulation. Blue: Positions of transmitters, red: triangular receiver arrays. The positions of the transmitters are that of a real ensemble of DAB transmitters in Italy whereas the places of the receivers are the result of a coverage optimization performed in the EU project 'ARGUS 3D'. Each of the five receiver arrays consists of three antennas located at the corners of an equilateral triangle with side lengths equal to the wavelength. So the complete number of sensors in the defined sense is* $L = 3 \times 5 = 15$.

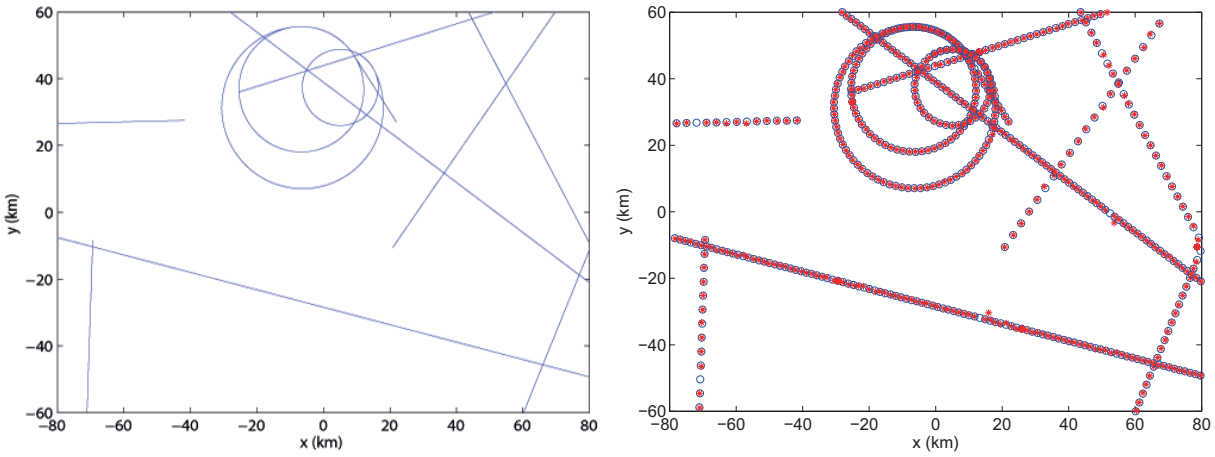

Figure 8: *Left: Simulated flight pathes of a number of aircrafts with velocities between 100 and 500 m/s with straight and curved trajectory segments. Observation time: 400 seconds at a temporal spacing of 2 seconds. A simulated receiver noise of - 10 dB relative to the signal power after range compression was added to the measurements. Right: Estimated flight paths using BOMP in combination with iterative fine estimation of positions. For each time frame the block sparse reconstruction is obtained for* $N = 17214$ *image points and totally* $\sum_{l=1}^{L} M^{(l)} = 4230$ *measurements.*

resolution cell become more and more correlated.

Fig. 3 shows the two-dimensional reconstruction of three lines cutting across with a zoom-factor 4 for both dimensions. The lines were assumed to be 'raw', i.e. with random phase along them. Still the basic pursuit denoising algorithm works exhibiting a much sharper image than the classical Hamming-windowed FFT. In fact, the CS-result shows super-resolution properties. Where the lines approach more than about a half of the resolution cell, their images mostly are melting to only one line. The CS image shows another interesting effect which can be detected also for imaging with real data: Instead of reproducing a solid line, we observe something

like a dotted line. We can explain this effect by the goal of CS to reduce the number of non-zero scattering points as much as possible while the measurements still have to be close to the assumed values $\mathbf{A}\widehat{\mathbf{x}}$. A densely dotted line can explain the measurements nearly as well as a solid line, the remaining error vanishes in the noise floor.

How does this approach work for real-world data? Fig. 4 shows ISAR imaging of a satellite. The data were obtained with the Fraunhofer space observation radar 'TIRA'. The CS-image of a detail of this satellite looks a little bit curious, since it consists only of points. It cannot be said that it looks 'better' than the conventional image processed with Hamming-windowing. Nevertheless, there appear two lines on the structure at left bottom which cannot be recognized in the classical image. We may call this 'super-resolution'. Perhaps it is the best to put the classical and the CS image together to get maximum information about the object.

6. Parametric models and autofocus

Sometimes the model used for CS is dependent on an unknown parameter vector $\boldsymbol{\vartheta}$, for instance in ISAR imaging when motion parameters are not known perfectly. This can be described either by a signal model depending on this parameter: $\mathbf{A}(\boldsymbol{\vartheta})\mathbf{x} = \mathbf{y} + \mathbf{n}$, $\mathbf{x}$ S-sparse, or by a parameter-dependent *compensation matrix* $\boldsymbol{\Phi}(\boldsymbol{\vartheta})$ which is applied to the measurements: $\boldsymbol{\Phi}(\boldsymbol{\vartheta})\mathbf{y} = \mathbf{A}\mathbf{x}$. In the latter approach $\boldsymbol{\Phi}(\boldsymbol{\vartheta})$ describes e.g. the compensation of phases induced by remaining motion errors. In both cases we would for instance like to minimize a linear combination between the ℓ_2-error and the ℓ_1-norm of $\|\mathbf{x}\|$ over $\mathbf{x}$ *and* $\boldsymbol{\vartheta}$, i.e. $\|\mathbf{A}(\boldsymbol{\vartheta})\mathbf{x} - \mathbf{y}\|_2^2 + \lambda\|\mathbf{x}\|_1 = \text{Min!}$, or $\|\mathbf{A}\mathbf{x} - \boldsymbol{\Phi}(\boldsymbol{\vartheta})\mathbf{y}\|_2^2 + \lambda\|\mathbf{x}\|_1 = \text{Min!}$, respectively. We have developed an iterative procedure for the latter problem improving the estimate of $\boldsymbol{\vartheta}$ in each step (by a second order Taylor approximation) and subsequently calculating new weight vectors for the enhancement of sparsity. A similar algorithm was proposed in [33].

The capability of our algorithm to estimate subsequently the unknown parameters driving the sparsity is illustrated in Fig. 5. A measurement with a thinned number of frequencies of a scene sparse in range was simulated imposing a quadratic phase error. The task of the autofocus algorithm is to remove the error phases by applying a chirp correction with subsequently adjusted slope. After a few iterations the recovery of the spiky scene is nearly perfect.

Another type of autofocus for two-dimensional object imaging based on sparse reconstruction and estimation of phase gradients is dealt in [34]. A simulation result is shown in Fig. 6.

7. Block sparsity: CS application to PCL

A passive coherent location (PCL) network is in many aspects different from classical radar sensors. The goal is to efficiently use the illumination from emitters of opportunity for the purpose of airspace surveillance by receiving the reflected waves by one or more passive units which may be dislocated [35]. This constellation is an involved version of multi-input multi-output (MIMO) radar with given, non-optimum positions of transmitters, a priori unknown

transmitted waveforms and distributed frequency bands. Each individual Tx-Rx pair measures primarily the bistatic distance to an object determining its position only partially, i.e. unknown remains the exact place on the surface of the bistatic ellipsoid. Secondly, the measurement of the Doppler frequency gives the sum of the radial velocities to Tx and Rx which does not restrict the possible positions on the ellipsoid directly [36].

For larger bistatic angles or different frequencies the individual Tx-Rx pairs of a PCL network cannot be assumed to work coherently. Consequently, the complex amplitudes related to the same target will be uncorrelated. This is exactly the situation of "block sparsity" [37], i.e. nearly all target positions on a search grid are empty with amplitudes equal to zero, whereas at the sparse points of present targets the amplitudes related to the different sensors are different and mostly non-zero. For this case CS theory offers strong tools for scene reconstruction.

Let us regard a general system of L linear sensors. Relating to PCL, the expression "sensor" stands for a transmitter (of opportunity) plus a 'co-located' array of receiving antennas, i.e. the complete aperture of the receiving array is small enough to guarantee phase coherency among the co-located receiving antennas. A PCL network is composed of a number of such elementary sensors. As a generalization of the scene as we have used before, now to each point $\omega_n \in \Omega$ there belongs an L-tuple of reflectivities $\left(\rho_n^{(1)}, \ldots, \rho_n^{(L)}\right)$ describing the amplitudes of a scatterer seen by the different sensors. As before, by choice of a representation basis $\mathbf{B}$ the reflectivities are transformed to coefficients $\left(x_n^{(1)}, \ldots, x_n^{(L)}\right)$, see Fig. 7 left. By collecting all coefficients to an $N \times L$ matrix $\mathbf{X}$ the scene now is characterized by

$$\mathbf{X} \;=\; \begin{pmatrix} x_1^{(1)} & \ldots & x_1^{(L)} \\ \ldots & \ldots & \ldots \\ x_N^{(1)} & \ldots & x_N^{(L)} \end{pmatrix}. \tag{2}$$

While the n-th row vector $\mathbf{x}[n]$ of this matrix describes the amplitudes at the scene point ω_n seen by the L sensors, the l-th column vector $\mathbf{x}^{(l)}$ reflects the amplitudes of all scene points as seen by sensor number l. Let $\boldsymbol{\xi}(\mathbf{X}) := (\ell_2(\mathbf{x}[1]), \ldots, \ell_2(\mathbf{x}[N]))^t$ be the vector of the Euclidean norms of the rows of $\mathbf{X}$, i. e. the square roots of the accumulated energies related to each scene point. A scene is called *block-sparse of order* S if the number of coefficients of $\boldsymbol{\xi}(\mathbf{X})$ larger than zero is equal or smaller than S. In our situation of airspace surveillance this means that not more than S airplanes are visible by at least one of the sensors.

Each of the L sensors performes measurements which are linear superpositions of the measurements at each scene point: $\mathbf{y}^{(l)} = \mathbf{A}^{(l)}\mathbf{x}^{(l)} + \mathbf{n}^{(l)}$. $\mathbf{A}^{(l)}$ is the sensing matrix related to the l-th sensor with dimension $M^{(l)} \times N$, if $M^{(l)}$ is the number of measurements of this sensor. $\mathbf{n}^{(l)}$ denotes the noise vector for sensor (l). The n-th column of $\mathbf{A}^{(l)}$ can be regarded as a *signal model* for the measurements performed by the sensor (l) if a normalized amplitude $\mathbf{x}_n^{(l)} = 1$ is present at scene point ω_n and all the other amplitudes are zero. Clearly, the complete ensemble of $M = \sum_{l=1}^{L} M^{(l)}$ measurements could be summarized in a single system of linear equations, but it is numerically better to handle the L equation systems separately.

In the literature there are presented a few algorithms for the reconstruction of the scene under the condition of this signal model and the assumption of block-sparsity. Examples are the *mixed ℓ_1/ℓ_2 optimization* minimizing $\|\boldsymbol{\xi}(\mathbf{X})\|_1$ under the constraints $\mathbf{y}^{(l)} = \mathbf{A}^{(l)}\mathbf{x}^{(l)}$ or the *Block Orthogonal Matching Pursuit* (BOMP) [37] as generalization of the OMP.

We have tested block-sparse recovery with a simulation series of a number of airplanes flying through the scene. Fig. 8 shows the simulated flight pathes and the results of sparse reconstruction using the BOMP algorithm with an additional component estimating the fine positions of the targets between the grid points. Both BOMP and position refinement aim to minimize the remaining energy sum over all sensors which cannot be explained by the actual assumed target positions.

8. Conclusions and outlook

We have presented various applications of CS to radar tasks. Many of them are very promising, open a new view to radar sensing and show new possibilities. Especially for spatial sparse sampling the benefits of CS are apparent, since each new proper, i.e. non-synthetic, spatial sample means an antenna, a T/R-module etc. and drives the costs of the system. Nevertheless, it's time to review the CS-techniques and to judge objectively the profit against classical methods. As a rule, sparse sampling should not reduce the accumulated signal-to-noise ratio (SNR), it should be the rule not to simply throw away samples which were gathered before, since this would reduce the potential accumulated SNR. It cannot be the aim, first to build up a system with given SNR specifications producing a certain data rate, and then to use only a part of the data to reduce the data rate again. There are other methods to produce a lower amount of data from the beginning without loosing SNR, e.g. the technique of illumination with a set of distinct frequencies simultaneously. Random choice of sampling times, frequencies or particularly aperture positions often can be carried out only once, namely during system design. For the rest of the system life time this choice has to be accepted.

In the very recent years, new ideas have come up, for instance algorithms driving down the rank of matrices analogue to the sparsity of vectors, adaptive dictionaries obtained by learning systems, or the handling of large sensor networks, which again could revolutionize the sensing techniques. So we expect that in a few years a new review of CS applied to radar would exhibit extremely interesting new techniques.

References

[1] D. Donoho, "Compressed sensing," *Information Theory, IEEE Transactions on*, vol. 52, no. 4, pp. 1289–1306, 2006.

[2] P. Gill, A. Wang, and A. Molnar, "The in-crowd algorithm for fast basis pursuit denoising," *Signal Processing, IEEE Transactions on*, vol. 59, no. 10, pp. 4595–4605, 2011.

[3] S. Mallat and Z. Zhang, "Matching pursuits with time-frequency dictionaries," *Signal Processing, IEEE Transactions on*, vol. 41, no. 12, pp. 3397–3415, 1993.

[4] D. Needell, J. Tropp, and R. Vershynin, "Greedy signal recovery review," in *Signals, Systems and Computers, 2008 42nd Asilomar Conference on*, 2008, pp. 1048–1050.

[5] J. H. G. Ender, "On compressive sensing applied to radar," *Signal Processing*, pp. 1402–1414, 2010.

[6] Y. Yanan, L. Chunsheng, and Y. Ze, "Parallel frequency radar via compressive sensing," in *Geoscience and Remote Sensing Symposium (IGARSS), 2011 IEEE International*, 2011, pp. 2696–2699.

[7] Y. He, X. Zhu, S. Zhuang, H. Li, and H. Hu, "Waveform optimization for compressive sensing radar imaging," in *Radar (Radar), 2011 IEEE CIE International Conference on*, vol. 2, 2011, pp. 1263–1266.

[8] I. Kyriakides, "Radar tracking performance when sensing and processing compressive measurements," in *Information Fusion (FUSION), 2010 13th Conference on*, 2010, pp. 1–8.

[9] G. Lellouch, R. Pribic, and P. Van Genderen, "Merging frequency agile ofdm waveforms and compressive sensing into a novel radar concept," in *Radar Conference, 2009. EuRAD 2009. European*, 2009, pp. 137–140.

[10] L. Pruente, "Application of compressed sensing to SAR/GMTI-data," in *Synthetic Aperture Radar (EUSAR), 2010 8th European Conference on*, 2010, pp. 1–4.

[11] Y. Yu, A. Petropulu, and H. Poor, "CSSF MIMO radar: Compressive-sensing and step-frequency based MIMO radar," *Aerospace and Electronic Systems, IEEE Transactions on*, vol. 48, no. 2, pp. 1490–1504, 2012.

[12] S. Gogineni and A. Nehorai, "Target estimation using compressive sensing for distributed MIMO radar," in *Signals, Systems and Computers (ASILOMAR), 2010 Conference Record of the Forty Fourth Asilomar Conference on*, 2010, pp. 793–797.

[13] M. Weiss,"Passive WLAN radar network using compressed sensing," Radar Systems (Radar 2012), IET International Conference on , vol., no., pp.1,6, 22-25 Oct. 2012

[14] P. Maechler, N. Felber, and H. Kaeslin, "Compressive sensing for wifi-based passive bistatic radar," in *Signal Processing Conference (EUSIPCO), 2012 Proceedings of the 20th European*, aug. 2012, pp. 1444 –1448.

[15] X. Peng, L. Chunsheng, and Y. Ze, "Effects of noise, sampling rate and signal sparsity for compressed sensing synthetic aperture radar pulse compression," in *Geoscience and Remote Sensing Symposium (IGARSS), 2011 IEEE International*, 2011, pp. 656–659.

[16] M. Tello Alonso, P. Lopez-Dekker, and J. Mallorqui, "A novel strategy for radar imaging based on compressive sensing," *Geoscience and Remote Sensing, IEEE Transactions on*, vol. 48, no. 12, pp. 4285–4295, 2010.

[17] X. X. Zhu and R. Bamler, "Demonstration of super-resolution for tomographic SAR imaging in urban environment," *Geoscience and Remote Sensing, IEEE Transactions on*, vol. 50, no. 8, pp. 3150–3157, 2012.

[18] ——, "Tomographic SAR inversion by l_1 -norm regularization the compressive sensing approach," *Geoscience and Remote Sensing, IEEE Transactions on*, vol. 48, no. 10, pp. 3839–3846, 2010.

[19] A. Budillon, A. Evangelista, and G. Schirinzi, "Three-dimensional SAR focusing from multipass signals using compressive sampling," *Geoscience and Remote Sensing, IEEE Transactions on*, vol. 49, no. 1, pp. 488–499, 2011.

[20] L. Li, D. Li, B. Liu, Q. Zhang, and L. Wei, "Three-aperture inverse synthetic aperture radar moving targets imaging processing based on compressive sensing," in *Instrumentation and Control Technology (ISICT), 2012 8th IEEE International Symposium on*, 2012, pp. 210–214.

[21] L. Zhang, M. Xing, C.-W. Qiu, J. Li, J. Sheng, Y. Li, and Z. Bao, "Resolution enhancement for inversed synthetic aperture radar imaging under low snr via improved compressive sensing," *Geoscience and Remote Sensing, IEEE Transactions on*, vol. 48, no. 10, pp. 3824–3838, 2010.

[22] M. Leigsnering, C. Debes, and A. Zoubir, "Compressive sensing in through-the-wall radar imaging," in *Acoustics, Speech and Signal Processing (ICASSP), 2011 IEEE International Conference on*, 2011, pp. 4008–4011.

[23] Y.-S. Yoon and M. Amin, "Through-the-wall radar imaging using compressive sensing along temporal frequency domain," in *Acoustics Speech and Signal Processing (ICASSP), 2010 IEEE International Conference on*, 2010, pp. 2806–2809.

[24] L. Wentai, W. Xiaodong, D. Jian, and L. Jianxin, "Ground penetating radar imaging algorithm of targets located in unknown subsurface environment based on compressive sensing," in *Information Science and Engineering (ICISE), 2010 2nd International Conference on*, 2010, pp. 6658–6661.

[25] K. Krueger, J. McClellan, and W. Scott, "3-D imaging for ground penetrating radar using compressive sensing with block-toeplitz structures," in *Sensor Array and Multichannel Signal Processing Workshop (SAM), 2012 IEEE 7th*, 2012, pp. 229–232.

[26] Y. Cao, R. Wu, J. Liu, and X. Lu, "Compressive sensing for ground penetrating radar imaging based on random filtering," in *Radar (Radar), 2011 IEEE CIE International Conference on*, vol. 2, 2011, pp. 1898–1901.

[27] T.-Y. Yu, L. Ding, and S. Ozturk, "Application of compressive sensing to refractivity retrieval with a network of radars," in *Radar Conference (RADAR), 2011 IEEE*, 2011, pp. 757–761.

[28] L. Anitori, M. Otten, W. Van Rossum, A. Maleki, and R. Baraniuk, "Compressive cfar radar detection," in *Radar Conference (RADAR), 2012 IEEE*, 2012, pp. 0320–0325.

[29] L. Anitori, M. Otten, and P. Hoogeboom, "False alarm probability estimation for compressive sensing radar," in *Radar Conference (RADAR), 2011 IEEE*, 2011, pp. 206–211.

[30] L. Anitori, "Compressive sensing and fast simulations," *Doctoral theses, Delft University of Technology, ISBN 978-94-6191-427-9*, 2012.

[31] X. X. Zhu and R. Bamler, "A fundamental bound for super-resolution with application to 3D SAR imaging," in *Urban Remote Sensing Event (JURSE), 2011 Joint*, 2011, pp. 181–184.

[32] S. jun Wu, L. Zhang, and M. dao Xing, "Super-resolution ISAR imaging via statistical compressive sensing," in *Radar (Radar), 2011 IEEE CIE International Conference on*, vol. 1, 2011, pp. 545–550.

[33] N. Onhon and M. Cetin, "A sparsity-driven approach for joint SAR imaging and phase error correction," *Image Processing, IEEE Transactions on*, vol. 21, no. 4, pp. 2075–2088, 2012.

[34] J. H. G. Ender, "Autofocusing ISAR images via sparse representation," in *Synthetic Aperture Radar, 2012. EUSAR. 9th European Conference on*, 2012, pp. 203–206.

[35] H. Kuschel and D. O"Hagan, "Passive radar from history to future," in *Radar Symposium (IRS), 2010 11th International*, 2010, pp. 1–4.

[36] M. Daun, Deghosting in passive air surveillance systems, in: Radar Symposium (IRS), 2010 11th International, 2010, pp. 1 –8..

[37] Y. Eldar, P. Kuppinger, and H. Bolcskei, "Block-sparse signals: Uncertainty relations and efficient recovery," *Signal Processing, IEEE Transactions on*, vol. 58, no. 6, pp. 3042 –3054, june 2010.

[38] X. Lv, G. Bi, and C. Wan, "The group lasso for stable recovery of block-sparse signal representations," *Signal Processing, IEEE Transactions on*, vol. 59, no. 4, pp. 1371 –1382, april 2011.